IOP Publishing Journal of Physics D: Applied Physics

J. Phys. D: Appl. Phys. **51** (2018) 355204 (14pp) https://doi.org/10.1088/1361-6463/aad47b

The effect of electron induced secondary electrons on the characteristics of low-pressure capacitively coupled radio frequency plasmas

B Horváth[1], J Schulze[2,3], Z Donkó[1] and A Derzsi[1,2,4]

[1] Institute for Solid State Physics and Optics, Wigner Research Centre for Physics, Hungarian Academy of Sciences, 1121 Budapest, Konkoly Thege Miklós str. 29-33, Hungary
[2] Department of Physics, West Virginia University, Morgantown, WV 26506, United States of America
[3] Institute of Electrical Engineering and Plasma Technology, Ruhr-University Bochum, 44780 Bochum, Germany

E-mail: derzsi.aranka@wigner.mta.hu

Received 26 May 2018, revised 6 July 2018
Accepted for publication 19 July 2018
Published 7 August 2018

Abstract

We investigate the effects of secondary electrons (SEs), induced by electrons impinging on the electrodes, on the characteristics of low-pressure single-frequency capacitively coupled plasmas (CCPs) by particle-in-cell/Monte Carlo collisions (PIC/MCC) simulations. In a recent PIC/MCC simulation study, that incorporated a realistic description of the electron-surface interaction, such electron-induced SEs (δ-electrons) were found to have a remarkable impact on the ionization dynamics and the plasma parameters in argon at 0.5 Pa and 6.7 cm gap between SiO_2 electrodes (Horváth *et al* 2017 *Plasma Sources Sci. Technol.* **26** 124001). At such low pressure and at high voltage amplitudes, the ion-induced SEs (γ-electrons) emitted at one electrode can reach the opposite electrode with high energies, where, depending on the surface material and surface conditions, they can induce the emission of a high number of δ-electrons, which can cause significant ionization and a higher plasma density. Here, we study the influence of δ-electrons on the ionization dynamics and plasma parameters at various pressures and voltage amplitudes, assuming different SE yields for ions (γ-coefficient) in single-frequency 13.56 MHz argon discharges. The emission of SEs by electron impact is found to be an important plasma-surface process at low pressures, between 0.5 Pa and 3 Pa. Both the gas pressure and the value of the γ-coefficient are found to affect the role of δ-electrons in shaping the discharge characteristics at different voltage amplitudes. Their effect on the ionization dynamics is most striking at low pressures, high voltage amplitudes and high values of the γ-coefficient. However, in the whole parameter regime investigated here, the realistic description of the electron-surface interaction significantly alters the computed plasma parameters, compared to results obtained based on a simple model for the description of the electron-surface interaction, widely used in PIC/MCC simulations of low-pressure CCPs.

Keywords: secondary electron emission, plasma-surface interaction, radio frequency plasmas, electron-surface processes

(Some figures may appear in colour only in the online journal)

[4] Author to whom any correspondence should be addressed.

1. Introduction

The interaction of plasma particles with the boundary surfaces in low-pressure capacitively coupled plasmas (CCPs) represents the basis for their applications in technological processes such as surface etching, deposition and sputtering [1–3]. In these applications, the plasma changes the nature of the surface exposed to particle bombardment, while at the same time, the surface also influences the characteristics of the plasma via various surface processes such as particle absorption, reflection and emission. The particle-in-cell approach [4, 5] combined with Monte Carlo type treatment of collision processes (known as the PIC/MCC method [6]) represents a powerful numerical method for the kinetic description of low-pressure CCPs [7–15], including the study of particle-surface interactions [16–20]. In PIC/MCC simulations of low-pressure CCPs, the description of the interaction of plasma particles with the boundary surfaces is generally implemented in a simplified manner. For heavy particles (only ions are traced in most studies), the assumption of a constant ion-induced secondary electron emission (SEE) coefficient is typical, which is independent of the incident particle's energy and angle, the electrode material and its surface conditions. However, the realistic energy and material dependent description of the SEE induced by heavy particles has been found to strongly influence the calculated plasma parameters in PIC/MCC simulations of low-pressure CCPs [21–26]. Such simulations typically assume a constant probability for the elastic reflection of the electrons at the electrodes, independently of the discharge conditions and properties of the boundary surfaces; other electron-surface processes are generally neglected, e.g. the emission of SEs due to electron impact, despite the fact that such electrons can significantly influence the discharge characteristics [21, 27, 28].

In a recent study the influence of the electron induced SEE from SiO_2 electrodes on the discharge characteristics in single-frequency (13.56 MHz) capacitive discharges has been investigated by PIC/MCC simulations in argon at 0.5 Pa [29]. In this study a realistic model for the description of the electron-surface interaction was developed, which took into account the elastic reflection and the inelastic backscattering of electrons, as well as the emission of electron induced SEs. The emission coefficients corresponding to these elementary processes were determined as a function of the energy and the angle of incidence of the primary electrons hitting the surface, taking the surface properties into account as well. The simulation results obtained by using this realistic model were compared to the results based on a simple model for the electron-surface interaction, which took into account only the elastic electron reflection at a constant probability of 0.2, independently of the discharge conditions and surface properties (typical assumption in PIC/MCC simulations of low-pressure CCPs, although the dependence of the electron reflection coefficient on the electrode material was shown theoretically as well [30]). It was found that the realistic description of the electron-surface interaction has a strong influence on the discharge characteristics at this low pressure, especially at high voltage amplitudes, where δ-electrons play a key role in the electron power absorption and ionization dynamics. Under such discharge conditions, the energetic ion-induced SEs (γ-electrons) cause the generation of a high number of electron-induced SEs upon impact at one of the electrodes during the time of local sheath collapse. Depending on the instantaneous local sheath voltage, these δ-electrons are accelerated into the plasma bulk, where they generate significant ionization, and can also induce SEE upon impact at the opposite electrode. Multiple reflections of both γ- and δ-electrons between the sheaths were also observed, as well as the generation of two beams of energetic electrons at each electrode within a RF period during sheath expansion and collapse, which both propagate into the plasma bulk. This electron power absorption and ionization dynamics was completely different from that obtained based on the simple description of the electron-surface interaction.

There are two well-studied discharge operation modes in low-pressure electropositive CCPs: the α-mode (at low pressures and driving voltages), where the ionization is dominated by electrons accelerated by the oscillating sheaths [31–35], and the γ-mode (at high pressures and/or voltages), where the ionization is dominated by SE avalanches inside the sheaths at the times of high sheath voltage [31]. In low-pressure electronegative gases other discharge operation modes are also possible [36, 37]. In [29], a discharge operation mode different from the α- and γ-modes has been reported for low-pressure CCPs, based on a model which takes into account the electron-surface interaction realistically. The realistic description of the electron-surface interaction was found to be essential at low pressures and high voltage amplitudes, suggesting that the electron-induced SEE has to be included in the discharge models in order to obtain realistic results.

The study in [29] was restricted to the relatively low pressure of 0.5 Pa and investigated the influence of the electron-induced SEs on the plasma density, the electron power absorption and the ionization dynamics for SiO_2 electrodes. The parameters of the model for the realistic description of the electron-surface interaction were set according to the characteristics of SiO_2 surfaces and an ion-induced SEE coefficient, γ, of 0.4 was assumed. Here, we study the effect of electron-induced SEs on the discharge characteristics in a wider pressure range between 0.5 Pa–3 Pa, for voltage amplitudes between 100 V–1500 V. Such discharge conditions (or even higher voltages) are typical in industrial applications, such as plasma etching, sputtering and plasma immersion ion implantation (PIII). Similarly to [29], here, the parameters of the realistic model for the electron-surface interaction reflect the properties of SiO_2 surfaces, however, we also vary the value of the ion-induced SEE coefficient, γ, between 0–0.4. Our aim is to provide an insight into the role of δ-electrons in the ionization dynamics under various discharge conditions in low-pressure CCPs. We aim to identify those discharge conditions where the realistic description of the electron-surface interaction is crucial in order to obtain reliable results from PIC/MCC simulations of CCPs. The results shown here provide a view also on the possible effect of δ-electrons on plasma parameters in discharges operated with electrodes other than SiO_2.

The paper is structured in the following way: in section 2 we describe the models used in the PIC/MCC simulations and introduce the discharge conditions covered. The simulation results are presented and discussed in section 3, while the conclusions are drawn in section 4.

2. Simulation setup and discharge conditions

We perform simulations of geometrically symmetric single-frequency CCPs in argon by using our 1d3v electrostatic PIC/MCC code [38]. A voltage waveform of $V(t) = V_0 \cos(2\pi ft)$ with $f = 13.56$ MHz is applied to one electrode, while the other electrode is grounded. The driving voltage amplitude, V_0, is varied between 100 V and 1500 V, while the neutral gas pressure is between 0.5 Pa and 3 Pa. The distance between the electrodes is 6.7 cm. We assume that the electrodes are made of the same material and the surface conditions of both electrodes are identical. The gas temperature is set to 400 K. The plasma particles traced in the simulations are electrons and Ar^+ ions. The cross sections for the electron-neutral and the ion-neutral collision processes are taken from [39–41].

The simulations are based on two different models:

(i) Model A incorporates a *simple description* of the electron-surface interaction, where we assume that the electrons are elastically reflected at the surfaces with a constant probability of 0.2 [42], independently of their energy and angle of incidence, and the other electron-surface processes are completely neglected. This approach has frequently been used in PIC/MCC simulations of low-pressure CCPs.

(ii) Model B incorporates a *realistic description* of the electron-surface interaction. This model, introduced in [29], is based on the conventional picture of the SEE, which assumes that the total yield of SEs (σ) due to primary electrons bombarding a surface consists of three components: elastically reflected electrons, inelastically backscattered electrons and electron-induced SEs (δ-electrons or true SEs). Therefore,

$$\sigma = \eta_e + \eta_i + \delta, \tag{1}$$

where η_e is the elastic reflection yield, η_i is the inelastic backscattering yield, and δ is the electron-induced SE yield. These emission coefficients, determined as proposed in [43], depend on the energy and the angle of incidence of the primary electrons and on the surface properties. The characteristics of the surface are taken into account via material specific input parameters, such as the maximum emission at normal incidence, the energy of the primary electron at maximum emission, etc. A detailed description of this approach is given in [29]. In this work the parameters of the realistic model for the electron-surface interaction are set in a way to reflect the properties of SiO_2 surfaces (see parameters listed in table 1 in [29]).

The total electron-induced SEE coefficient, σ and the partial emission coefficients, η_e, η_i and δ used in model B are shown in figure 1 as a function of the incident electron energy, ε, at normal incidence. At low electron energies σ increases rapidly with ε, reaches a maximum value of $\sigma_{max} = 2.5$ at a primary electron energy of $\varepsilon_{max} = 400$ eV, then slowly decreases towards high energies. This dependence of σ on ε is in agreement with the experimental trends observed for different surface materials [44–46]. The values of σ_{max} and ε_{max} vary over a wide range for different materials: σ_{max} is smaller than 2 for most metals and can reach values higher than 10 for some oxides; ε_{max} is generally between 100 eV and 1000 eV [44, 46]. The properties of the surface, as well as the angle of incidence of the electrons affect the SE yield: for oblique impact, the values of σ_{max} and ε_{max} are significantly increased [44].

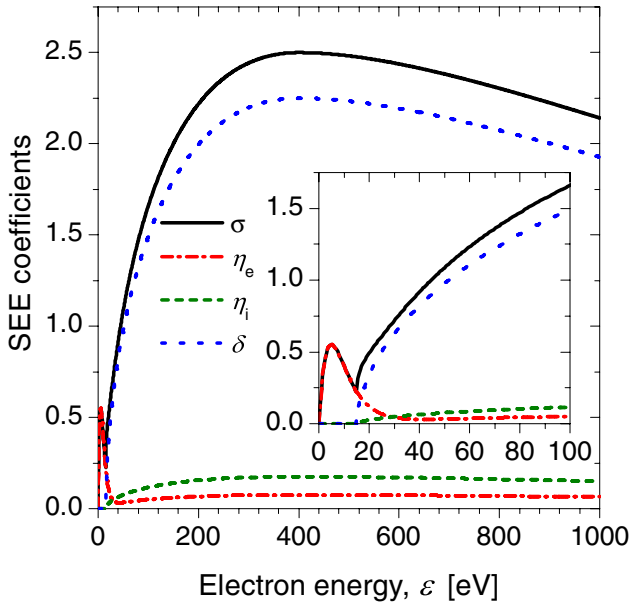

Figure 1. The total electron induced SEE coefficient (σ) and the partial emission coefficients of the elastic reflection (η_e), inelastic backscattering (η_i) and electron-induced SEE (δ) as a function of the incident electron energy, ε, at normal incidence for SiO_2 surfaces [29]. The inset shows the same quantities in the low-energy domain. Reproduced from [29]. © IOP Publishing Ltd. All rights reserved.

We use constant values for the ion induced SEE coefficient, γ, in the simulations. The value of γ is varied between 0 and 0.4. As our main goal is to illustrate here the effect of δ-electrons on the plasma parameters under various discharge conditions, we do not take into account the energy-dependence of the SE yield for ions [47, 48]. Simulations are performed based on model A (with a simple description of the electron-surface interaction) and model B (with a realistic description of the electron-surface interactions) for all discharge conditions.

All computations have been carried out using a spatial grid with 500–2500 points and 5×10^3–6×10^4 time steps within the RF period. These parameters have been selected to fulfill the stability criteria of the computational method. The number of superparticles in the simulations was $\approx 10^5$. The simulation results have been obtained by averaging over 10^4 cycles of the RF period.

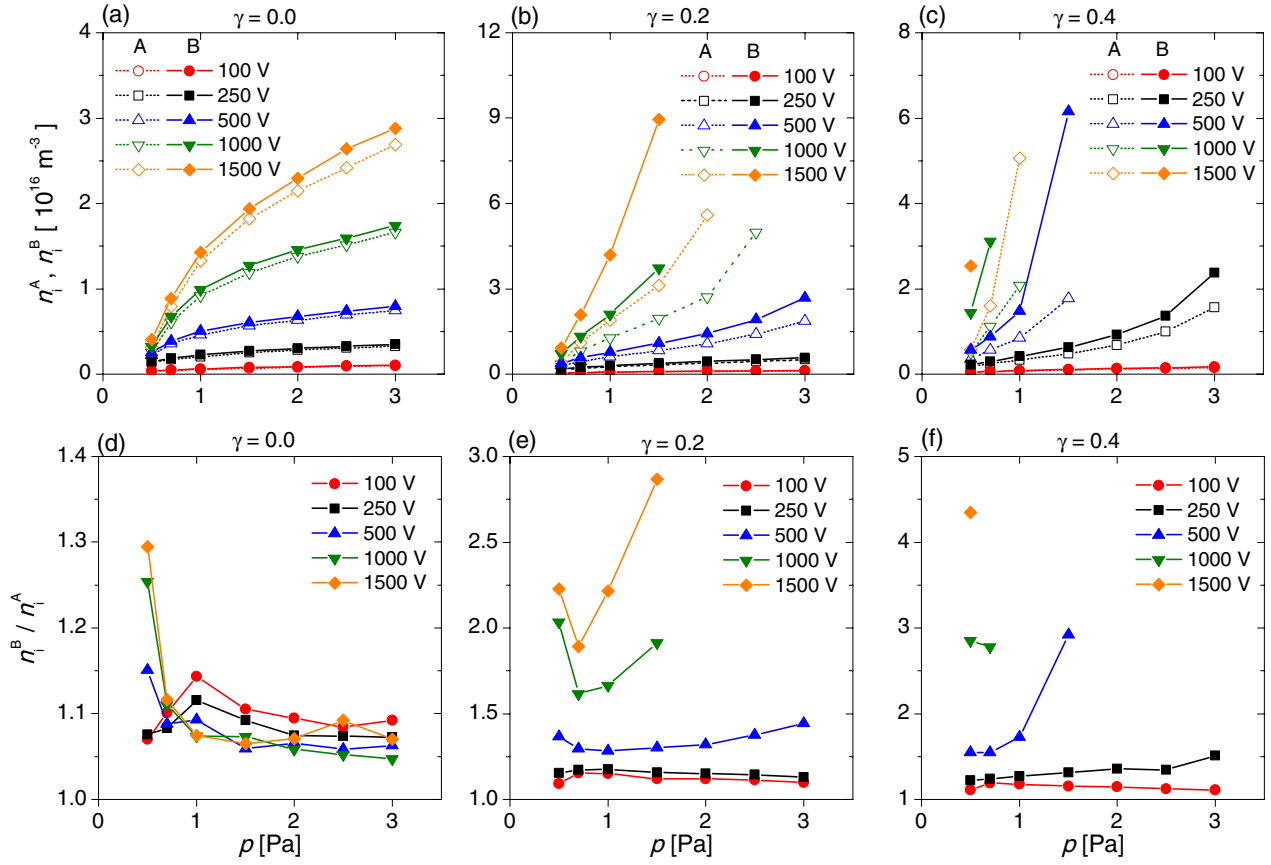

Figure 2. The central ion densities (top row) obtained from model A and model B, n_i^A (open symbols) and n_i^B (filled symbols), respectively, and the n_i^B/n_i^A ratio of the central ion densities (bottom row) as a function of the gas pressure, for different driving voltage amplitudes and for various values of the ion-induced SEE coefficient: $\gamma = 0.0$ ((a), (d)), $\gamma = 0.2$ ((b), (e)) and $\gamma = 0.4$ ((c), (f)).

3. Results

Figure 2, in panels (a)–(c) in the top row, shows the ion density in the center of the discharge, obtained from model A and model B, n_i^A (open symbols) and n_i^B (filled symbols), respectively, as a function of the gas pressure, p, for different driving voltage amplitudes, V_0, and for various values of the ion-induced SEE coefficient, γ. The gas pressure is varied between 0.5 and 3 Pa. The voltage amplitude is changed from 100 V up to 1500 V. Such high (or even higher) voltage amplitudes are often used for plasma etching, PIII and plasma sputtering. Simulations are performed by assuming γ-coefficients of 0 (neglecting the SEE due to ions), 0.2 (assuming surfaces characterized by intermediate ion-induced SEE property), and 0.4 (considering surfaces with high SEE due to ions). The panels (d)–(f) in the bottom row of figure 2 display the n_i^B/n_i^A ratio of the central ion densities. Both models predict, for all V_0 and for all values of γ, an increase of the central ion density with increasing the gas pressure. At all pressures, for a given V_0 and γ, the plasma density is higher in the simulations based on model B compared to model A. The lowest densities are obtained for $\gamma = 0$, where the emission of SEs due to ion impact is neglected in the simulations (figure 2(a)). At the lowest voltage amplitude of $V_0 = 100$ V, both models predict that the plasma density changes only slightly with the pressure. At the highest voltage amplitude of $V_0 = 1500$ V an increase by a factor of 8.6 based on model A, and 7.2 based on model B, is obtained by increasing the pressure from 0.5 Pa to 3 Pa. For $\gamma = 0$, both models A and B result in similar plasma densities for a given pressure and voltage amplitude. This can be seen also in panel (d), where the n_i^B/n_i^A ratio is about 1.1 independently of p, except at the lowest pressure of 0.5 Pa, where for voltage amplitudes above 500 V a maximum of 1.3 times higher plasma density is obtained based on model B compared to model A. The simulations based on model B show that at 0.5 Pa, at high voltage amplitudes ($V_0 > 500$ V) a high flux of electron induced SEs (δ-electrons) is initiated at the electrodes during the time of sheath collapse (see later in figure 8) and these δ-electrons significantly contribute to the total ionization in the discharge (see later in figure 7(a)). For instance, at $V_0 = 1500$ V about 27% of the total ionization is directly caused by δ-electrons. This effect is completely neglected in the conventional description of the electron-surface interaction in PIC/MCC models of CCPs (model A), where only the elastic electron reflection is included in the model.

By taking into account the SEE due to ion impact in the simulations and assuming $\gamma = 0.2$, at low voltage amplitudes (100 V, 250 V) similar values for the peak ion densities are obtained from both models (figure 2(b)) and n_i^B/n_i^A is about 1.1 independently of p (figure 2(e)). For $V_0 = 500$ V, n_i^B/n_i^A first decreases (for $p < 1$ Pa), then slightly increases

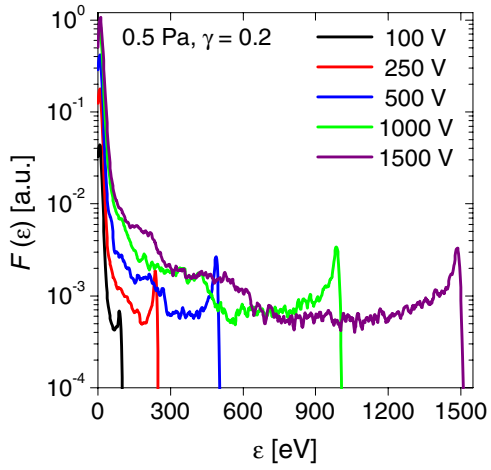

Figure 3. The energy distribution of the electrons at the electrodes, $F(\varepsilon)$, obtained from simulations based on model B at 0.5 Pa, $\gamma = 0.2$, for different driving voltage amplitudes. The distributions are given in arbitrary units, which are the same for all curves, i.e. their ratios express the ratios of the true fluxes.

at higher pressures; at 3 Pa, about a 1.5 times higher plasma density is obtained based on model B compared to model A. At high voltage amplitudes (1000 V, 1500 V), the plasma density rapidly increases with increasing the pressure based on both models; at $V_0 = 1500$ V n_i^A changes by a factor of about 8, while n_i^B changes by a factor of about 10, when the pressure is increased from 0.5 Pa to 1.5 Pa (figure 2(b)). At the lowest pressure of 0.5 Pa, the n_i^B/n_i^A density ratio is above 2 for high voltage amplitudes (figure 2(e)). Similarly to the case of $V_0 = 500$ V, n_i^B/n_i^A first decreases by increasing the pressure (to 0.7 Pa), then steeply increases towards high pressures, where the plasma density obtained based on model B significantly exceeds that obtained based on model A. A maximum n_i^B/n_i^A density ratio of about 2.7 is obtained at 1.5 Pa, 1500 V (figure 2(e)). For $\gamma = 0.2$ the simulations based on model B diverge above ~1.5 Pa for high voltage amplitudes, while the simulations based on model A reach convergence at higher pressures as well. The divergence of the simulations at high pressures and high voltage amplitudes is related to the efficient multiplication of the SEs emitted at the electrodes. These electrons are accelerated by the instantaneous sheath voltage and can reach high energies in the sheaths at high driving voltages. Significant ionization can be induced by these electrons, as well as the formation of electron avalanches at high pressures, which lead to the drastic increase of the plasma density. This behavior actually corresponds to experimentally observed instabilities (e.g. arcing) at similar discharge conditions.

For $\gamma = 0.2$, the simulations based on model B show that at the lowest pressure of 0.5 Pa, at high voltage amplitudes ($V_0 > 500$ V), besides δ-electrons γ-electrons also contribute to the emission of SEs (see later in figure 8). These δ-electrons play a key role in the ionization dynamics, having a contribution to the total ionization close to 50% at high voltages (see later in figure 7). In model B, the higher the voltage amplitude is, the more SEs are induced by electron impact at the electrodes due to the high SEE coefficient at high electron energies (the electron-induced SEE coefficient, δ, is 2.25 at 400 eV, see figure 1). The energy distribution of the electrons impacting the electrodes is shown in figure 3 for different driving voltage amplitudes at 0.5 Pa and $\gamma = 0.2$. γ-electrons gain higher energies at higher voltages and induce the emission of more δ-electrons at the opposite electrode. As a result, the plasma density obtained based on model B is higher than that obtained based on model A, which leads to $n_i^B/n_i^A > 2$ at 1000 V and 1500 V, at 0.5 Pa. By increasing the pressure, the flux of SEs due to electron impact at the electrodes decreases, which results in less ionization directly induced by δ-electrons (see later in figure 7(b)). This leads to a decrease of the n_i^B/n_i^A density ratio (see figure 2(e)). A further increase of the pressure results in an even lower flux of δ-electrons from the electrodes; however, these electrons are more efficiently multiplied within the sheaths at higher pressures, which finally leads to a drastic increase of the plasma density obtained based on model B (figure 2(b)), and, as a consequence, the increase of the n_i^B/n_i^A density ratio with the pressure (figure 2(e)).

The largest differences between the plasma densities calculated based on model A and model B are obtained for $\gamma = 0.4$ (figure 2(c)). At the highest voltage amplitude of 1500 V and the lowest pressure of 0.5 Pa investigated here, the ratio of the central ion densities $n_i^B/n_i^A = 4.4$ (figure 2(f)). For $\gamma = 0.4$, the simulations based on model B diverge above ~1.5 Pa for 500 V; at voltage amplitudes of 1000 V and 1500 V, convergence of the simulations based on model B is restricted to the domain of even lower gas pressures. Again, for simulations based on model A, convergence can be achieved in a wider pressure range.

We note that γ-electrons also have an important role in the ionization dynamics. First of all, these electrons can enhance the ionization due to their collisional multiplication. Secondly, γ-electrons themselves can induce emission of SEs (δ-electrons), which also generate ionization and can induce electron avalanches in the sheath, thus, increase the plasma density in the discharge. However, this latter effect is only described in model B, in which the electron-induced SEE is taken into account via the realistic model for the electron-surface interaction. Therefore, only in model B (and not in model A) there is a strong collisional multiplication of SEs inside the sheaths, which is most pronounced at high voltages and pressures. Thus n_i^B/n_i^A increases as a function of pressure only for $\gamma \neq 0$ (see figures 2(e) and (f) compared to figure 2(d)).

These results show that the realistic description of the electron-surface interaction in the discharge model can strongly affect the calculated plasma densities, especially at low pressures and high voltage amplitudes. The difference between the results obtained from model A and model B is more pronounced at high values of γ, i.e. for surfaces that are characterized by a high SE yield due to ions (heavy particles). This is well visible also in figure 4, which shows the time-averaged charged particle density profiles in the discharge gap, obtained from simulations based on model A and model B at 0.5 Pa, for different voltage amplitudes (100 V, 500 V, 1000 V) and for various values of γ (0, 0.2, 0.4). The difference between the peak charged particle densities obtained from model B compared to model A increases both by increasing the voltage amplitude at a given γ (see panels of figure 4 in a given column

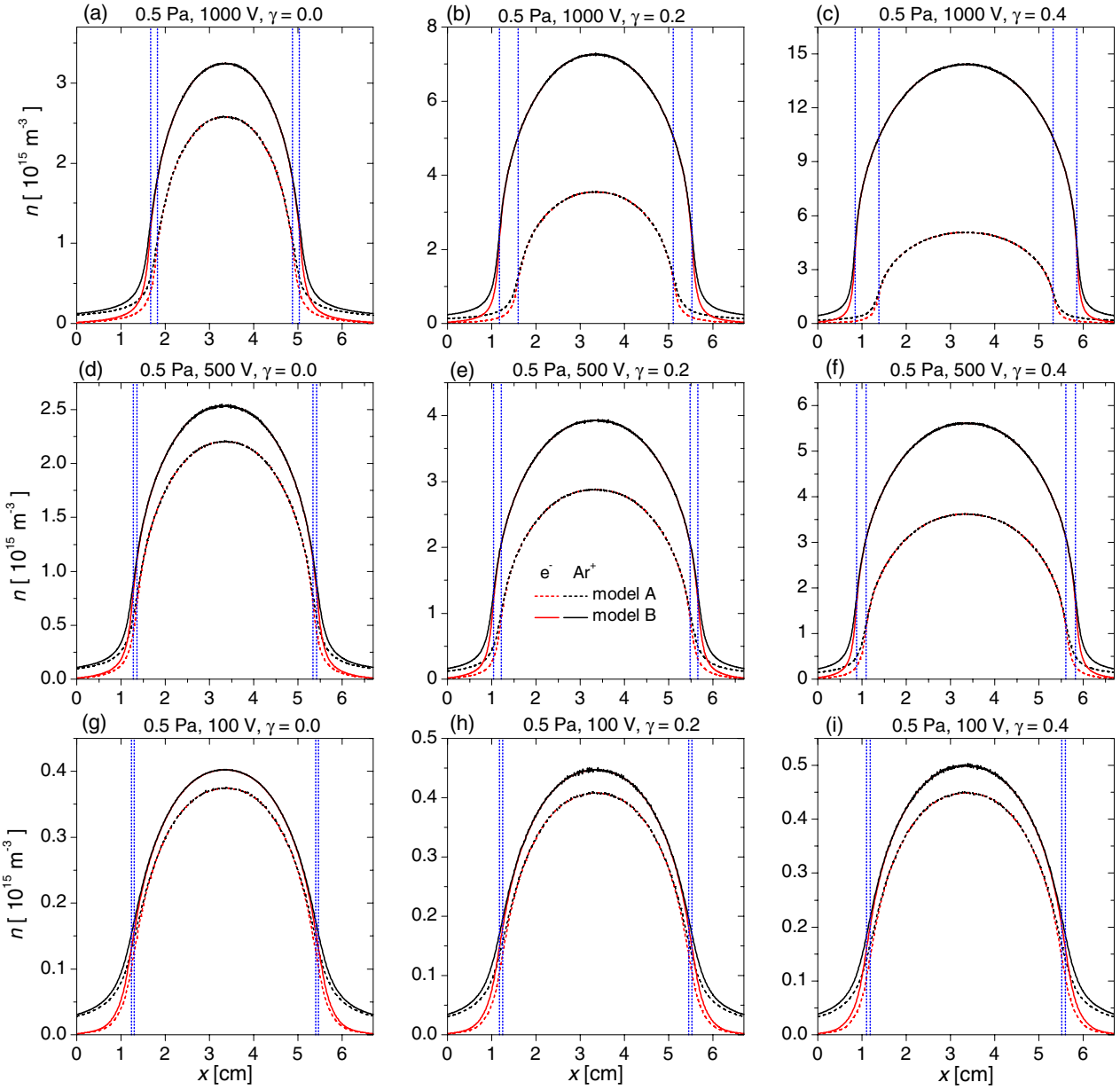

Figure 4. Time-averaged charged particle density distributions obtained from model A (dashed lines) and model B (continuous lines) for driving voltage amplitudes of 1000 V (first row), 500 V (second row) and 100 V (third row), for different ion-induced SE yields: $\gamma = 0.0$ (first column), $\gamma = 0.2$ (second column) and $\gamma = 0.4$ (third column). The vertical dotted lines mark the maximum sheath lengths [49] at both electrodes, for both models A and B.

from bottom to top) and by increasing the value of γ at a given voltage amplitude (see panels of figure 4 in a given row from left to right). This figure also reveals the difference in the sheath lengths obtained from models A and B under various discharge conditions. The positions of the maximum sheath lengths are marked in the figure by vertical dotted lines at both electrodes, for both models A and B. The sheath lengths are calculated in the simulations by using the criterion proposed by Brinkmann [49]. While at the low voltage amplitude of 100 V the sheath length is only slightly affected by changing γ (bottom row), at $V_0 = 1000$ V a significant decrease of the sheath length is found in model B compared to model A, and the difference increases by increasing γ from 0 to 0.4 (top row). Increasing the voltage amplitude at a given γ also leads to a decrease of the sheath length in simulations based on model B compared to model A (see panels of figure 4 in a given column from bottom to top). The differences in the sheath lengths are most pronounced at the highest voltage amplitude and the highest value of γ, 1000 V and 0.4, respectively, shown here (panel top right). For higher voltage amplitudes even larger differences are obtained. These effects can influence the ion properties, such as the ion flux and the energy of ions at the electrodes. This is illustrated in figure 5, which shows the flux of ions (first row), Γ_i, and the mean energy of ions (second row), $\langle E_i \rangle$, at the electrodes as a function of the gas pressure for different driving voltage amplitudes and for various values of the ion-induced SEE coefficient, γ. The flux of the ions at the electrodes obtained from model B is higher than that

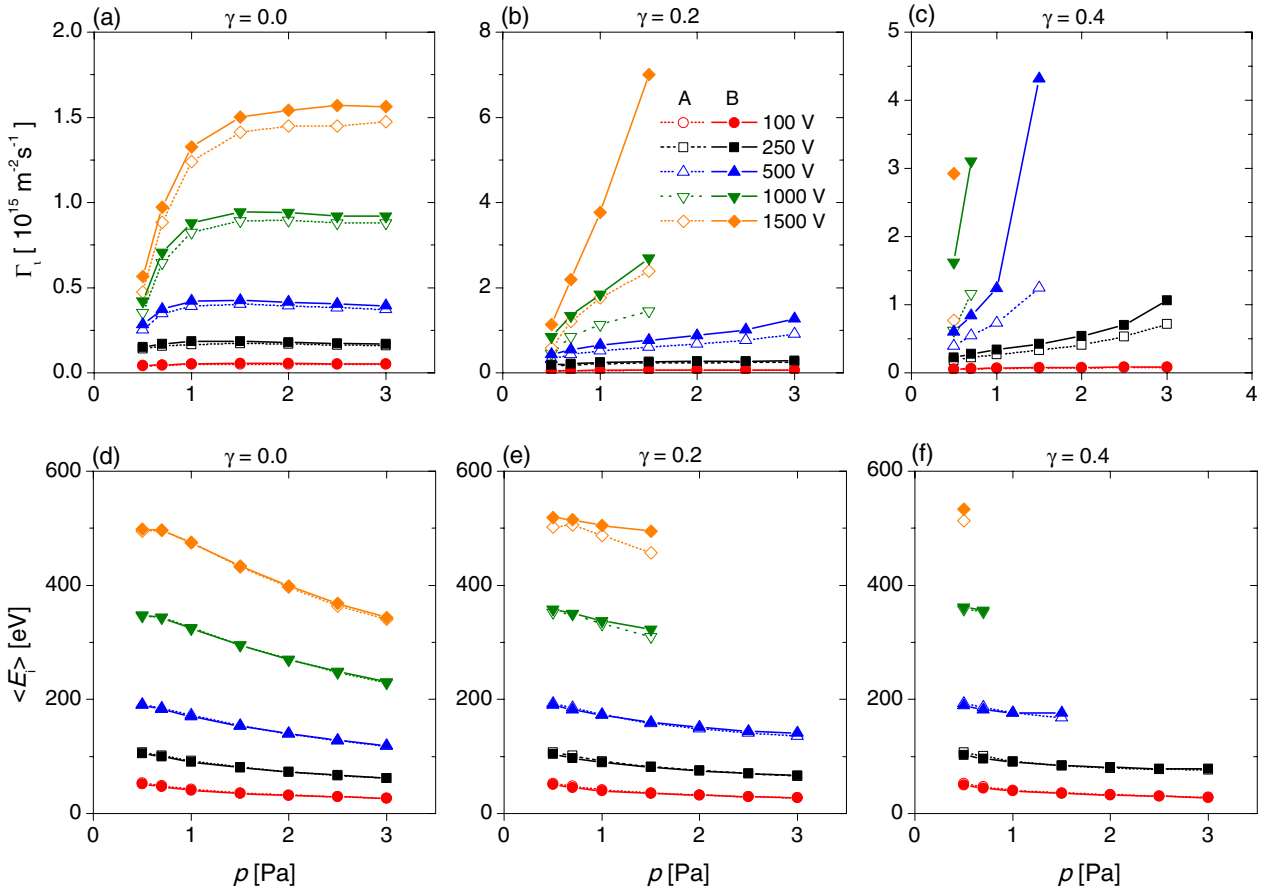

Figure 5. The ion flux (top row), Γ_i, and the mean ion energy (bottom row), $\langle E_i \rangle$, at the electrodes obtained from model A (open symbols) and model B (filled symbols), as a function of the gas pressure, for different driving voltage amplitudes and for different values of the ion-induced SEE coefficient: $\gamma = 0.0$ ((a), (d)), $\gamma = 0.2$ ((b), (e)) and $\gamma = 0.4$ ((c), (f)).

obtained from model A at all pressures, for all voltage amplitudes and for all values of γ, which can be explained by the higher plasma densities obtained from model B compared to model A (see figure 2). The mean energy of ions at the electrodes obtained from model B is only slightly higher than that obtained from model A at high voltage amplitudes and only in the regime of higher pressures, despite the fact that significant differences in the sheath lengths are obtained at high voltage amplitudes at low pressures as well (see results for 0.5 Pa in figure 4). The sheath is smaller in simulations based on model B compared to model A for all discharge conditions investigated here. However, at low pressures the ions reach the electrodes without collisions in the sheath. As a result, the smaller sheath lengths obtained based on model B lead to less collisions involving ions in the sheaths only at higher pressures. Therefore, ions reach the electrodes at higher energies in model B compared to model A only at high voltage amplitudes at the highest pressures investigated here.

In [29] a detailed analysis of the simulation results (performed by using models A and B at 0.5 Pa, 13.56 MHz, 1000 V, 6.7 cm electrode gap, $\gamma = 0.4$) has revealed that the SEE induced by electrons at the electrodes (included only in model B) is the fundamental process behind the higher plasma densities and the shorter sheath lengths obtained from model B compared to model A. For the above discharge conditions model B resulted in about 2.75 times higher plasma density than model A, and completely different electron power absorption and ionization dynamics were obtained in the two different models for the same discharge conditions. The simulation based on model A showed discharge operation in the classical α-mode [31], where the ionization is dominated by the electrons that are accelerated at the expanding sheath edge; one beam of energetic electrons is generated at both electrodes during a RF period at the time of sheath expansion, which propagates through the bulk at low pressures and causes ionization. In the simulations based on model B, however, two beams of energetic electrons were found at both electrodes during a RF period, and consequently, two separate maxima in the spatio-temporal distribution of the ionization rate were observed at both electrodes during a RF period [29]: (i) strong ionization at the expanding sheath edge (beam I) and (ii) additional ionization during sheath collapse (beam II, weaker compared to beam I). These beams are shown by arrows in panel (c) of figure 6 for the conditions investigated in [29]. The beams II were found to be mainly composed of δ-electrons, which play a key role also in the α-mode ionization at the expanding sheath edge (beams I) [29].

Figure 6 illustrates the effects of the voltage amplitude and the value of γ on the ionization dynamics at a constant pressure of 0.5 Pa: the spatio-temporal distributions of the

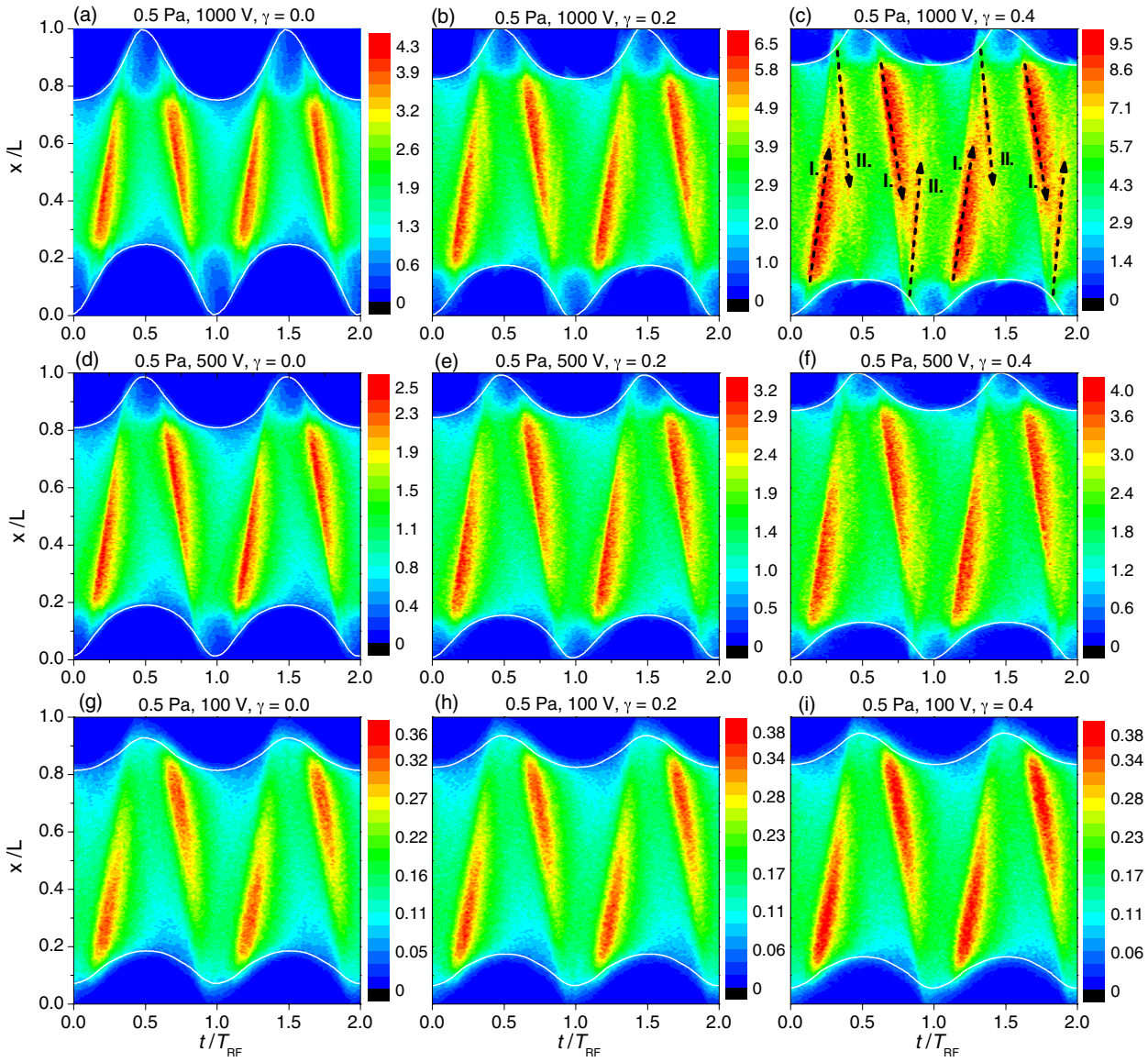

Figure 6. Spatio-temporal distribution of the total ionization rate obtained from model B at $p = 0.5$ Pa, for driving voltage amplitudes of 1000 V (first row), 500 V (second row) and 100 V (third row), for different values of the ion-induced SEE coefficient: $\gamma = 0.0$ (first column), $\gamma = 0.2$ (second column) and $\gamma = 0.4$ (third column). The white lines mark the sheath edges adjacent to each electrode. The color scales are given in units of 10^{20} m^{-3} s^{-1}.

ionization rate obtained from model B are shown for voltage amplitudes of 100 V, 500 V and 1000 V, for γ-coefficients of 0, 0.2 and 0.4. The sheath edge positions (shown as white lines in the plots at both electrodes) are calculated based on the criterion proposed by Brinkmann [49]. Compared to the spatio-temporal distribution of the ionization rate shown in panel (c) for 1000 V and $\gamma = 0.4$, where two beams due to ionization by energetic electrons can be clearly identified during a RF period at both electrodes, the ionization dynamics is affected by both changing γ and V_0. A decrease of γ (from right lo left in a given row), as well as a decrease of V_0 (from top to bottom in a given column) leads to less and less noticeable beams launched shortly before the time of sheath collapse at both electrodes (beams II). At low voltage amplitudes (e.g. bottom row, $V_0 = 100$ V) and low values of γ (e.g. first column, $\gamma = 0$) beams II cannot be identified in the spatio-temporal maps of the ionization rate. However, δ-electrons still play an important role in the ionization dynamics under such conditions as well, as it can be seen in figure 7, which shows the contribution of the different electron species (δ-electrons, γ-electrons, and bulk electrons) to the total ionization obtained from model B as a function of the gas pressure, for different voltage amplitudes and for different values of γ.

We note that the term *bulk electrons* refers to all the electrons that are not created at the electrodes, i.e. electrons that are neither γ-electrons nor δ-electrons. Thus, the electrons created in ionization collisions between the γ- or δ-electrons and the atoms of the background gas are also considered bulk electrons. The panels in the first column of figure 7 show the results obtained for $\gamma = 0$. The SEE due to ions is neglected, therefore, the contribution of γ-electrons to the ionization is zero for all pressures and all voltage amplitudes (panel (d)),

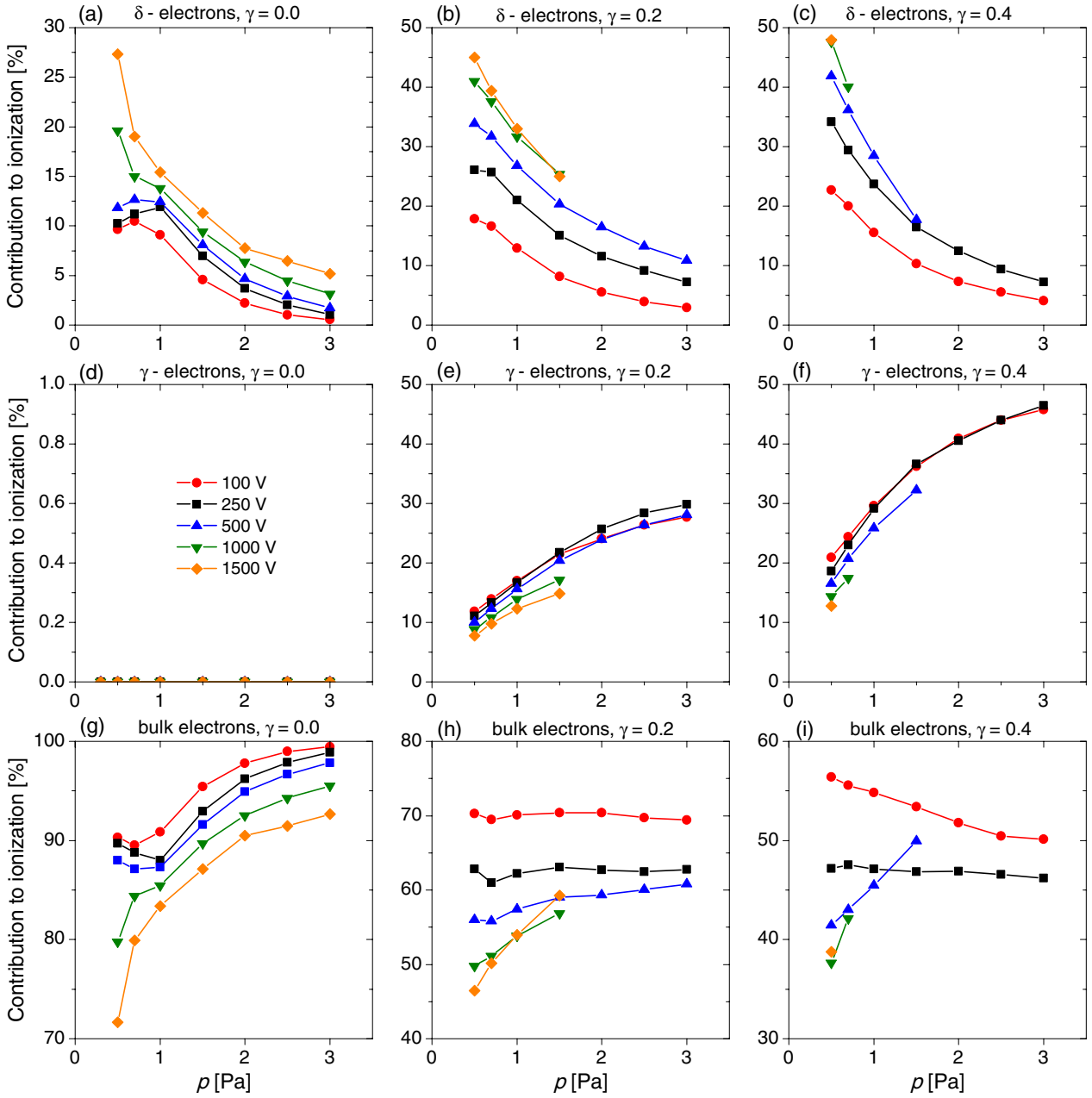

Figure 7. The contributions of δ-electrons (first row), γ-electrons (second row) and bulk electrons (third row) to the total ionization obtained from model B, as a function of the gas pressure, for different driving voltage amplitudes and various values of the ion-induced SEE coefficient: $\gamma = 0.0$ (first column), $\gamma = 0.2$ (second column) and $\gamma = 0.4$ (third column).

only δ-electrons and bulk electrons cause ionization (panels (a) and (g)). At 0.5 Pa and $V_0 = 100$ V, δ-electrons have a contribution of about 10% to the total ionization. By increasing the voltage amplitude, their contribution to the total ionization increases to ~12% at 500 V, ~20% at 1000 V and ~27% at 1500 V (figure 7(a)), despite the fact that the spatio-temporal maps of the ionization rate do not exhibit beams II for such discharge conditions (figure 6, first column). Under such conditions, δ-electrons are mainly generated by bulk electrons at the time of sheath collapse at both electrodes. This can be seen for the powered electrode side in the panels in the first column of figure 8, which displays the total flux of the outgoing electron induced SEs at the powered electrode as well as the contributions of δ-electrons, γ-electrons and bulk electrons to the generation of this flux at 0.5 Pa, for different values of γ (0, 0.2 and 0.4) and for different voltage amplitudes (100 V, 500 V and 1000 V). At $\gamma = 0$, the flux of δ-electrons emitted at the electrodes increases by increasing the driving voltage amplitude (see the blue curves of the first column of figure 8, from bottom to top). These δ-electrons generated by bulk electrons during the time of sheath collapse are accelerated by the expanding sheath, propagate into the bulk and cause ionization (in beams I). Therefore, under such discharge conditions the δ-electrons enhance the ionization in the α-mode electron power absorption. The effect of δ-electrons on the ionization dynamics is even larger than what can be concluded based on

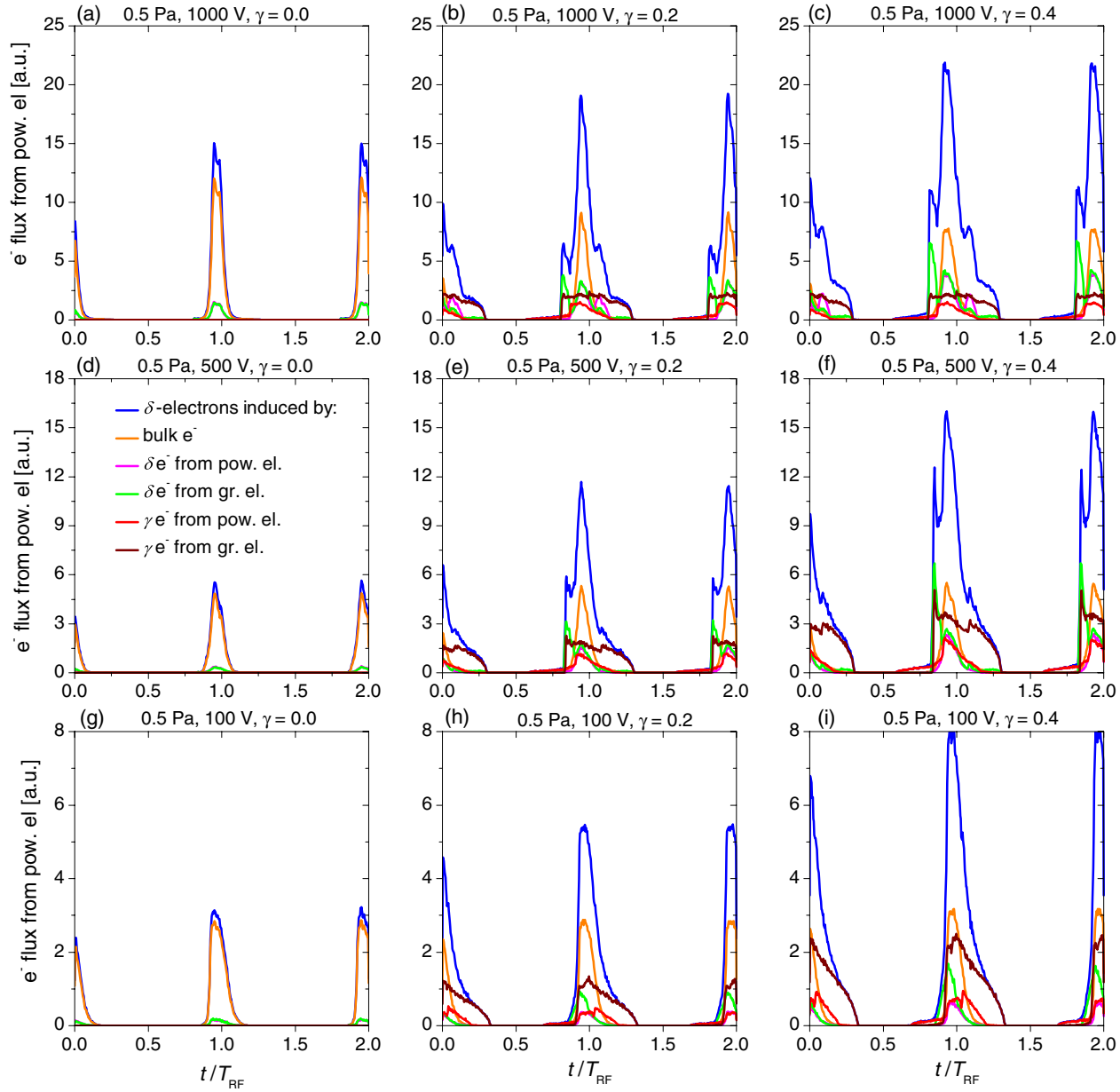

Figure 8. Electron-induced SE (δ-electron) flux from the powered electrode and the contribution of bulk electrons, δ-electrons and γ-electrons (differentiated to two components according to which electrode they originate from) to this SE flux, obtained from model B for driving voltage amplitudes of 1000 V (first row), 500 V (second row) and 100 V (third row), for different values of the ion-induced SEE coefficient: $\gamma = 0.0$ (first column), $\gamma = 0.2$ (second column) and $\gamma = 0.4$ (third column).

the plots in the first row of figure 7. A large number of bulk electrons are generated by δ-electrons (ionization), and these bulk electrons can also induce significant ionization. This can be considered as an indirect effect of δ-electrons on the ionization.

Similarly, by increasing γ at the lowest voltage amplitude of $V_0 = 100$ V at 0.5 Pa, the contribution of δ-electrons to the ionization increases to $\sim$18% at $\gamma = 0.2$ and $\sim$23% at $\gamma = 0.4$ (figures 7(a)–(c)), while beams II cannot be observed in the spatio-temporal plots of the ionization rate for these cases (figure 6, last row). Under such conditions, besides bulk electrons, δ-electrons, as well as γ-electrons (emitted at both electrodes) induce emission of SEs at a given electrode. For instance, δ-electrons and γ-electrons emitted at the grounded electrode also have a significant contribution to the generation of SEs at the powered electrode (see figures 8(h) and (i)). However, at such low voltages, these δ- and γ-electrons created at the grounded electrode can reach the powered electrode and induce SEE only during the time of sheath collapse, they cannot overcome the residual sheath potential when the sheath is partially collapsed at the powered electrode. The δ-electrons created by these electrons, as well as those created by bulk electrons during the time of sheath collapse are accelerated by the expanding sheath at the powered electrode and contribute significantly to the ionization in the α-mode.

At a given pressure, the contribution of δ-electrons to the ionization increases with the voltage amplitude as well as with the value of γ (figure 7, first row). By taking into account

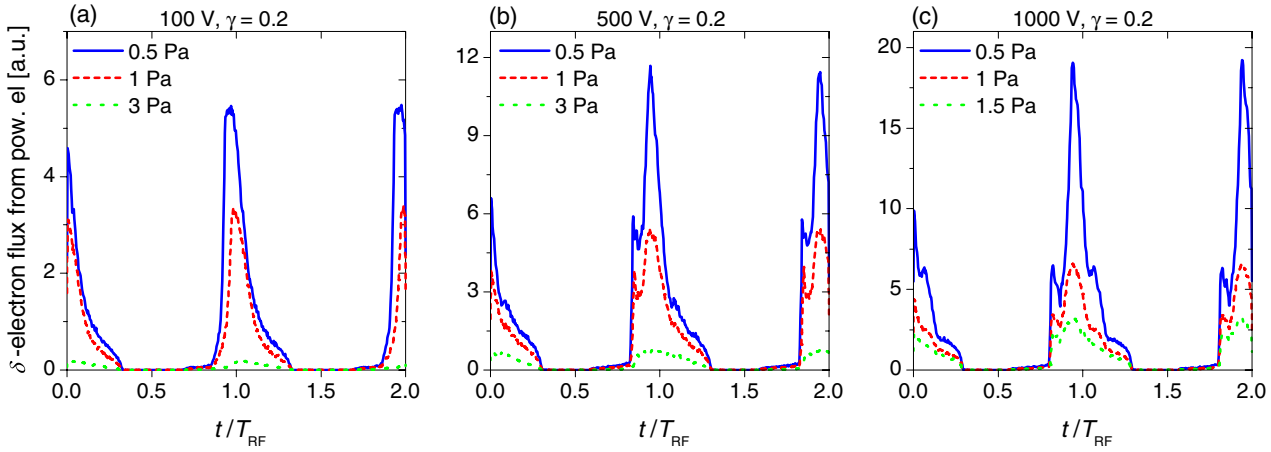

Figure 9. Electron-induced SE (δ-electron) flux from the powered electrode, obtained from model B for driving voltage amplitudes of 100 V (a), 500 V (b) and 1000 V (c), at different pressures. $\gamma = 0.2$.

the SEE due to ion impact in the simulations, δ-electrons are generated by γ-electrons as well (see emission fluxes for 0.5 Pa in figure 8). At low pressures and high voltage amplitudes the γ-electrons generated at one electrode and accelerated by the high instantaneous sheath voltage at this electrode can overcome the residual sheath potential at the other electrode, hit the electrode at high energies and induce the emission of a high number of δ-electrons. The higher the value of γ is, the more γ-electrons are emitted at the electrodes, and the more δ-electrons are induced by γ-electron impact at a fixed pressure and voltage amplitude. By increasing the voltage amplitude, the γ-electrons can reach the opposing electrode with higher energies, which results in more SEs emitted by electron impact, due to the higher SEE coefficients at higher electron energies (see figure 1). These δ-electrons induced by γ-electrons are then accelerated into the bulk by the residual sheath voltage and induce significant ionization in the bulk (beams II). This effect, as well as the influence of δ-electrons on the ionization in the α-mode leads to the key role of these electrons in the electron power absorption and ionization dynamics at low pressures and high voltage amplitudes. At 0.5 Pa, for $\gamma = 0.2$ and $\gamma = 0.4$, close to 50% of the total ionization is directly generated by δ-electrons at high voltage amplitudes (figures 7(b) and (c)). For such discharge conditions, beams II can clearly be identified in the spatio-temporal distribution of the ionization rate (see figures 6(b), (c) and (f)). Under such conditions the δ-electrons generated at one electrode can reach the opposite sheath, where, depending on the instantaneous local sheath potential they are reflected into the bulk or reach the electrode. Those δ-electrons that reach the electrode can also contribute to the emission of SEs and these δ-electrons play a crucial role in the formation of ionizing beams (beams II) launched shortly before the sheath collapses at both electrodes (see the dominant contribution of δ-electrons originated at the grounded electrode to the SEE at the powered electrode before the time of sheath collapse in panels (b), (c), (e) and (f) of figure 8). The δ-electrons (as well as the other electrons comprised in beams II) that are reflected from the sheath can traverse the bulk region and arrive to the other sheath, where they can hit the respective electrode, or can be reflected back into the bulk again by the instantaneous sheath electric field (figure 6(c)). Such multiple reflection of the beam electrons was found to enhance the ionization in the discharge [29].

The contribution of δ-electrons to the ionization decreases with increasing the gas pressure at a given voltage amplitude and γ, except the case of low voltage amplitudes ($V_0 \leqslant 500$ V) at $\gamma = 0$ (figure 7(a)). For the lowest voltage amplitude of $V_0 = 100$ V at $\gamma = 0$, the contribution of δ-electrons to the ionization first increases with the gas pressure (below 1 Pa, reaching a maximum contribution of about 11%), then decreases towards higher gas pressures (figure 7(a)); at the highest pressure of 3 Pa, less than 1% of the total ionization is directly generated by δ-electrons. A similar trend can also be observed for voltage amplitudes of 250 V and 500 V. At $\gamma = 0$, at the lowest pressures of 0.5 Pa and at low voltage amplitudes, δ-electrons are mainly generated by bulk electrons at the time of sheath collapse at both electrodes (figure 8(g)). Under such conditions, the collisional multiplication of these escaping electrons is not efficient. By slightly increasing the gas pressure (up to 0.7 Pa), the contribution of δ-electrons to the ionization increases due to the more frequent collisions. However, as the pressure is even further increased, the flux of electron-induced SEs from the electrodes decreases due to the decrease of the incident electron energy, but the multiplication of these δ-electrons becomes more and more efficient. All the electrons that originate from this multiplication, i.e. a collision between a δ-electron and an atom of the background gas are considered bulk electrons. In other words, the more efficient the multiplication of the δ-electron beam is, the larger portion of the beam will consist of bulk electrons, by definition. As a consequence of these effects, the contribution of δ-electrons to the ionization strongly decreases, while that of bulk electrons strongly increases with the pressure (figure 7, first column). A similar scenario, i.e. a decrease of the contribution of δ-electrons to the ionization with the gas pressure, is found at high voltage amplitudes as well at $\gamma = 0$. However, at high voltage amplitudes, the highest contribution of δ-electrons to the ionization is found at the lowest pressure of 0.5 Pa (27% at $V_0 = 1500$ V). At 0.5 Pa, a large flux of δ-electrons

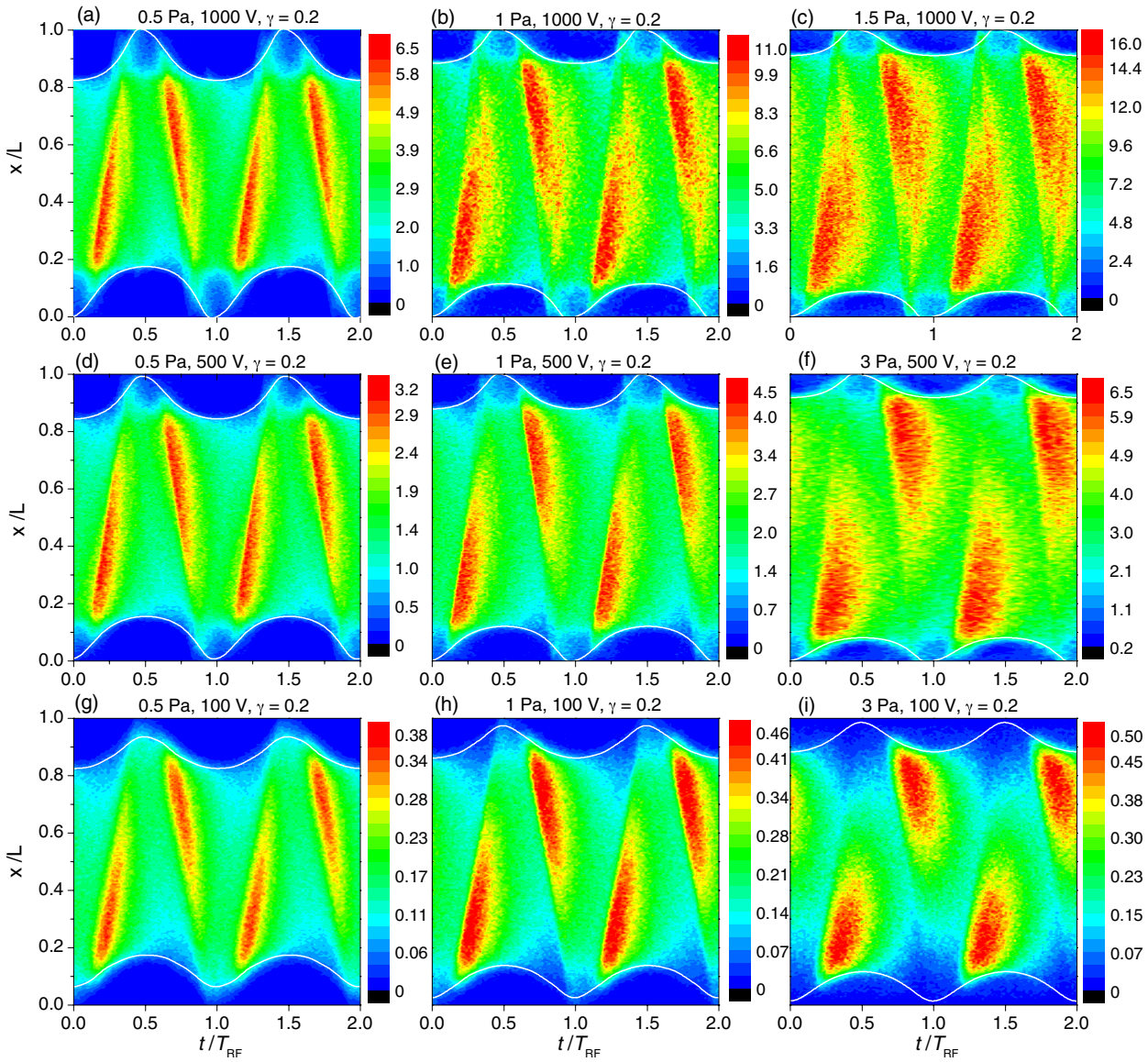

Figure 10. Spatio-temporal distribution of the total ionization rate obtained from model B at different pressures between 0.5 Pa–3 Pa (columns from left to right), for driving voltage amplitudes of 1000 V (first row), 500 V (second row) and 100 V (third row), for $\gamma = 0.2$. The white lines mark the sheath edges adjacent to each electrode. The color scales are given in units of 10^{20} m^{-3} s^{-1}.

from the electrodes is induced by bulk electrons at the time of sheath collapse at high voltage amplitudes (see figure 8(a) for 1000 V). This large flux of δ-electrons and the ionization induced by these electrons compensates the negative effect of the less efficient multiplication of δ-electrons at low pressures on the ionization dynamics.

For nonzero values of γ, the contribution of δ-electrons to the ionization decreases with increasing the pressure at all voltage amplitudes. Under such conditions the ion-induced SEs also have a significant contribution to the total ionization. At the lowest pressure of 0.5 Pa, for $\gamma = 0.2$, about 10% of the ionization is generated by γ-electrons, while for $\gamma = 0.4$ this value increases to ∼20% (see figures 7(e) and (f)), since the number of γ-electrons in the discharge cell increases. At a given voltage amplitude and γ, the importance of γ-electrons to the ionization increases with the gas pressure, due to the more efficient collisional multiplication of these electrons at high pressures. Due to the more frequent collisions, the electrons reach the electrodes at lower energies, which leads to a decrease of the number of SEs emitted by electron impact at the electrodes, and, therefore, to a decrease of the contribution of δ-electrons to the ionization by increasing the pressure. The flux of SEs emitted by electron impact at the powered electrode (δ-electron flux) is shown in figure 9 for different driving voltage amplitudes and for different pressures at $\gamma = 0.2$.

The influence of the pressure on the ionization dynamics is illustrated in figure 10, which shows the spatio-temporal distribution of the total ionization rate obtained from model B at different pressures between 0.5 Pa and 3 Pa (columns from left to right) and for different driving voltage amplitudes (100 V, 500 V, and 1000 V, rows from bottom to top) at $\gamma = 0.2$. The white lines in the plots mark the positions of the sheath edge at both electrodes [49]. The increase of the pressure at a given voltage amplitude leads to an enhancement of

the ionization due to γ-electrons (figures 7(e) and (f)) and discharge operation in a hybrid α-γ mode (see figure 10, second row, for $\gamma = 0.2$ and $V_0 = 500$ V). Despite the fact that the number of δ-electrons emitted at the electrodes decreases with the pressure (see figure 9), at high voltage amplitudes these electrons are efficiently multiplied at high pressures. This can be seen in the first row of figure 10 for 1000 V voltage amplitude for pressures between 0.5 Pa and 1.5 Pa. The bulk electrons created in electron-impact ionization by δ-electrons are also efficiently multiplied, which leads to the increase of the contribution of bulk electrons to the total ionization with increasing pressure at high voltage amplitudes (figures 7(h) and (i)).

For a certain pressure and γ value, the contribution of γ-electrons to the ionization decreases with increasing voltage amplitude (figures 7(e) and (f)). This can be explained by the energy-dependence of the SEE induced by electrons: the higher the energy of the γ-electrons is, the higher the probability that they induce one or more δ-electrons at the electrodes, which increases the contribution of δ-electrons (and indirectly the contribution of bulk electrons) to the ionization. Therefore, the contribution of γ-electrons apparently decreases with increasing V_0.

4. Conclusions

In this work we studied the influence of electron induced SEs (δ-electrons) on the electron power absorption and ionization dynamics and plasma parameters by PIC/MCC simulations at different pressures and voltage amplitudes, assuming various SE yields for ions (γ-coefficient) in single-frequency 13.56 MHz argon discharges. We used the realistic model for the description of the electron-surface interaction introduced in [29], which takes into account the elastic reflection and the inelastic backscattering of electrons, as well as the emission of electron induced SEs as a function of the energy and the angle of incidence of the electrons arriving at the electrodes (model B). The simulation results obtained by using this model were compared to those obtained by using a simple model for the description of the electron-surface interaction (model A), widely used in PIC/MCC simulations of low-pressure CCPs.

Compared to the study in [29], here we covered a wider pressure range between 0.5 Pa–3 Pa, and voltage amplitudes between 100 V–1500 V. Such discharge conditions (or even higher voltages) are typical in industrial applications, such as plasma etching, sputtering and PIII. Similar to [29], the parameters of the realistic model for the electron-surface interaction were set to reflect the properties of SiO_2 surfaces, however, we varied the value of the ion-induced SEE coefficient, γ, between 0 and 0.4.

At all pressures, for a given voltage amplitude and γ, higher plasma densities were obtained from model B compared to model A. The highest differences between the plasma densities calculated based on the different models were obtained for $\gamma = 0.4$. At the highest voltage amplitude of 1500 V and the lowest pressure of 0.5 Pa investigated here, at $\gamma = 0.4$, a 4.4 times higher plasma density was obtained from the model which describes the electron-surface interaction in a realistic way (model B) compared to the results obtained by using a simple model for the description of the electron-surface interaction (model A). The different implementations of the description of the electron-surface interaction in the simulations were found to affect the calculated ion properties, such as the ion flux and mean energy of ions at the electrodes.

The ionization dynamics obtained from simulations based on model B was found to be influenced by both changing the voltage amplitude, V_0, and the ion-induced SEE coefficient, γ, at a given pressure. The contribution of δ-electrons to the ionization increases with the voltage amplitude as well as with the value of γ. The δ-electrons generated by γ-electrons when the sheath is partially collapsed at a given electrode are accelerated into the bulk by the residual sheath voltage and induce significant ionization in the bulk. The δ-electrons emitted at the time of sheath collapse and accelerated by the expanding sheath contribute to the ionization in the α-mode. These effects lead to the key role of δ-electrons in the electron power absorption and ionization dynamics at low pressures and high voltage amplitudes, at high values of γ. At 0.5 Pa, for $\gamma = 0.2$ and $\gamma = 0.4$, close to 50% of the total ionization is directly generated by δ-electrons at high voltage amplitudes. δ-electrons can have a significant contribution (up to about 30%) to the ionization under low V_0 and/or low γ discharge conditions as well. δ-electrons influence the ionization dynamics indirectly as well: a large number of bulk electrons are generated by δ-electrons, and these bulk electrons can also induce significant ionization in the discharge.

The contribution of δ-electrons to the ionization decreases with increasing the gas pressure at a given voltage amplitude and γ. Due to the more frequent collisions at high pressures, the electrons reach the electrodes at lower energies, which leads to a decrease of the number of SEs emitted by electron impact at the electrodes, therefore, to a decrease of the contribution of δ-electrons to the ionization.

These results show that the emission of SEs by electron impact is an important plasma-surface process at low pressures between 0.5 Pa–3 Pa. We find that the effect of δ-electrons on the ionization dynamics is most pronounced at low pressures, high voltage amplitudes and high values of the γ-coefficient. However, the realistic description of the electron-surface interaction (model B) was found to lead to different plasma parameters compared to results obtained based on a simple model for the description of the electron-surface interaction (model A) within the whole parameter regime investigated here.

Besides δ-electrons, γ-electrons generated by ion impact at the electrodes were also found to play an important role in the discharge under the conditions investigated here. At low pressures and high voltage amplitudes, such electrons have a significant contribution to the emission of δ-electrons. While a realistic model was implemented to describe the SEE induced by electron impact at the electrodes, constant γ-coefficients were used in this work to describe the ion-induced SEE. However, the value of the γ-coefficient largely depends on the discharge conditions and the surface properties. The investigation of the combined effect of using a realistic model for the electron-surface interaction, as well as for describing the interaction of heavy particles with the surfaces will be addressed in a future study.

Acknowledgments

This work was supported by the US NSF grant No. PHY. 1601080, by the German Research Foundation (DFG) within the frame of the collaborative research centre SFB-TR 87, by the Hungarian National Research, Development and Innovation Office via grants K-119357 and PD-121033 and by the J Bolyai Research Fellowship of the Hungarian Academy of Sciences (AD).

ORCID iDs

J Schulze https://orcid.org/0000-0001-7929-5734
Z Donkó https://orcid.org/0000-0003-1369-6150
A Derzsi https://orcid.org/0000-0002-8005-5348

References

[1] Lieberman M A and Lichtenberg A J 2005 *Principles of Plasma Discharges and Materials Processing* 2nd edn (New York: Wiley)
[2] Makabe T and Petrović Z 2006 *Plasma Electronics: Applications in Microelectronic Device Fabrication* (London: Taylor & Francis)
[3] Chabert P and Braithwaite N 2011 *Physics of Radio-Frequency Plasmas* (Cambridge: Cambridge University Press)
[4] Birdsall C K and Langdon A B 1985 *Plasma Physics via Computer Simulation* (New York: McGraw-Hill)
[5] Hockney R W and Eastwood J W 1981 *Computer Simulation Using Particles* (New York: McGraw-Hill)
[6] Birdsall C K 1991 *IEEE Trans. Plasma Sci.* **19** 65
[7] Diomede P, Capitelli M and Longo S 2005 *Plasma Sources Sci. Technol.* **14** 459
[8] Matyash K, Schneider R, Taccogna F, Hatazarna A, Longo S, Capitelli M, Tskhakaya D and Bronold F X 2007 *Contrib. Plasma Phys.* **47** 595
[9] Verboncoeur J P 2005 *Plasma Phys. Control. Fusion* **47** A231
[10] Donkó Z 2011 *Plasma Sources Sci. Technol.* **20** 24001
[11] Bruneau B, Gans T, O'Connell D, Greb A, Johnson E V and Booth J P 2015 *Phys. Rev. Lett.* **114** 125002
[12] Bruneau B, Lafleur T, Booth J-P and Johnson E 2016 *Plasma Sources Sci. Technol.* **25** 025006
[13] Greb A, Niemi K, O'Connell D and Gans T 2013 *Appl. Phys. Lett.* **103** 244101
[14] Liu Y-X, Zhang Q-Z, Liu Y, Song Y-H, Bogaerts A and Wang Y-N 2012 *Appl. Phys. Lett.* **101** 114101
[15] Gudmundsson J T, Kawamura E and Lieberman M A 2013 *Plasma Sources Sci. Technol.* **22** 035011
[16] Donkó Z, Schulze J, Hartmann P, Korolov I, Czarnetzki U and Schuengel E 2010 *Appl. Phys. Lett.* **97** 081501
[17] Schulze J, Donkó Z, Schuengel E and Czarnetzki U 2011 *Plasma Sources Sci. Technol.* **20** 045007
[18] Korolov I, Derzsi A, Donkó Z and Schulze J 2013 *Appl. Phys. Lett.* **103** 064102
[19] Lafleur T, Chabert P and Booth J P 2013 *J. Phys. D: Appl. Phys.* **46** 13520
[20] Greb A, Gibson A R, Niemi K, O'Connell D and Gans T 2015 *Plasma Sources Sci. Technol.* **24** 044003
[21] Braginsky O, Kovalev A, Lopaev D, Proshina O, Rakhimova T, Vasilieva A, Voloshin D and Zyryanov S 2012 *J. Phys. D: Appl. Phys.* **45** 015201
[22] Bojarov A, Radmilović-Radjenović M and Petrović Z Lj 2010 *Proc. 20th ESCAMPIG (Novi Sad, Serbia, 13–17 July 2010) p* 2.38
Bojarov A, Radmilović-Radjenović M and Petrović Z Lj 2010 *Publ. Astron. Obs. Belgrade* **89** 131
Bojarov A, Radmilović-Radjenović M and Petrović Z Lj 2012 *Proc. 65th Annual Gaseous Electronics Conf. (Austin, Texas, 22–26 October 2012)*
Bojarov A, Radmilović-Radjenović M and Petrović Z Lj 2014 *Proc. 27th Summer School and Int. Symp. on the Physics of Ionized Gases (Belgrade, Serbia, 26–29 August 2014)*
[23] Radmilović-Radjenović M and Petrović Z Lj 2009 *Eur. Phys. J.* D **54** 445
[24] Derzsi A, Korolov I, Schüngel E, Donkó Z and Schulze J 2015 *Plasma Sources Sci. Technol.* **24** 034002
[25] Hannesdottir H and Gudmundsson J T 2016 *Plasma Sources Sci. Technol.* **25** 055002
[26] Daksha M, Derzsi A, Wilczek S, Trieschmann J, Mussenbrock T, Awakowicz P, Donkó Z and Schulze J 2017 *Plasma Sources Sci. Technol.* **26** 085006
[27] Khrabrov A V, Kaganovich I D, Ventzek P L G, Ranjan A and Chen L 2015 *Plasma Sources Sci. Technol.* **24** 054003
[28] Korolov I, Derzsi A, Donkó Z, Schuengel E and Schulze J 2016 *Plasma Sources Sci. Technol.* **25** 015024
[29] Horváth B, Daksha M, Korolov I, Derzsi A and Schulze J 2017 *Plasma Sources Sci. Technol.* **26** 124001
[30] Bronold F X and Fehske H 2017 *Plasma Phys. Control. Fusion* **59** 014011
[31] Belenguer P and Boeuf J P 1990 *Phys. Rev.* A **41** 4447
[32] Vender D and Boswell R 1992 *Vac. Sci. Technol.* A **10** 1331
[33] Schulze J, Heil B G, Luggenhölscher D, Mussenbrock T, Brinkmann R P and Czarnetzki U 2008 *J. Phys. D: Appl. Phys.* **41** 042003
[34] Turner M M and Hopkins M B 1992 *Phys. Rev. Lett.* **69** 3511
[35] Schulze J, Donkó Z, Lafleur T, Wilczek S and Brinkmann R P 2018 *Plasma Sources Sci. Technol.* **27** 055010
[36] Schulze J, Derzsi A, Dittmann K, Hemke T, Meichsner J and Donkó Z 2011 *Phys. Rev. Lett.* **107** 275001
[37] Liu Y-X, Schuengel E, Korolov I, Donkó Z, Wang Y-N and Schulze J 2016 *Phys. Rev. Lett.* **116** 255002
[38] Donkó Z, Schulze J, Czarnetzki U, Derzsi A, Hartmann P, Korolov I and Schüngel E 2012 *Plasma Phys. Control. Fusion* **54** 124003
[39] Phelps A V http://jilawww.colorado.edu/~avp/collision_data/ unpublished
[40] Phelps A V 1994 *J. Appl. Phys.* **76** 747
[41] Phelps A V 1991 *J. Phys. Chem. Ref. Data* **20** 557
[42] Kollath R 1956 *Encyclopedia of Physics* vol XXI, ed S Flügge (Berlin: Springer) p 264
[43] Sydorenko D 2006 Particle-in-cell simulations of electron dynamics in low pressure discharges with magnetic fields *PhD Thesis* University of Saskatchewan, Saskatoon, Canada
[44] Vaughan J R M 1989 *IEEE Trans. Electron Devices* **36** 1963
[45] Ruzic D, Moore R, Manos D and Cohen S 1982 *J. Vac. Sci. Technol.* **20** 1313
[46] Seiler H 1983 *J. Appl. Phys.* **54** R1–8
[47] Phelps A V and Petrović Z Lj 1999 *Plasma Sources Sci. Technol.* **8** R21
[48] Sobolewski M 2017 *Proc. 70th Annual Gaseous Electronics Conf. (Pittsburgh, PA, 6–10 November 2017)*
[49] Brinkmann R P 2007 *J. Appl. Phys.* **102** 093303